Science Advances
AAAS

Supplementary Materials for

Switchable immune modulator for tumor-specific activation of anticancer immunity

Yu Zhao, Yu-Qing Xie, Simon Van Herck, Sina Nassiri, Min Gao, Yugang Guo, Li Tang*

*Corresponding author. Email: li.tang@epfl.ch

Published 10 September 2021, *Sci. Adv.* **7**, eabg7291 (2021)
DOI: 10.1126/sciadv.abg7291

This PDF file includes:

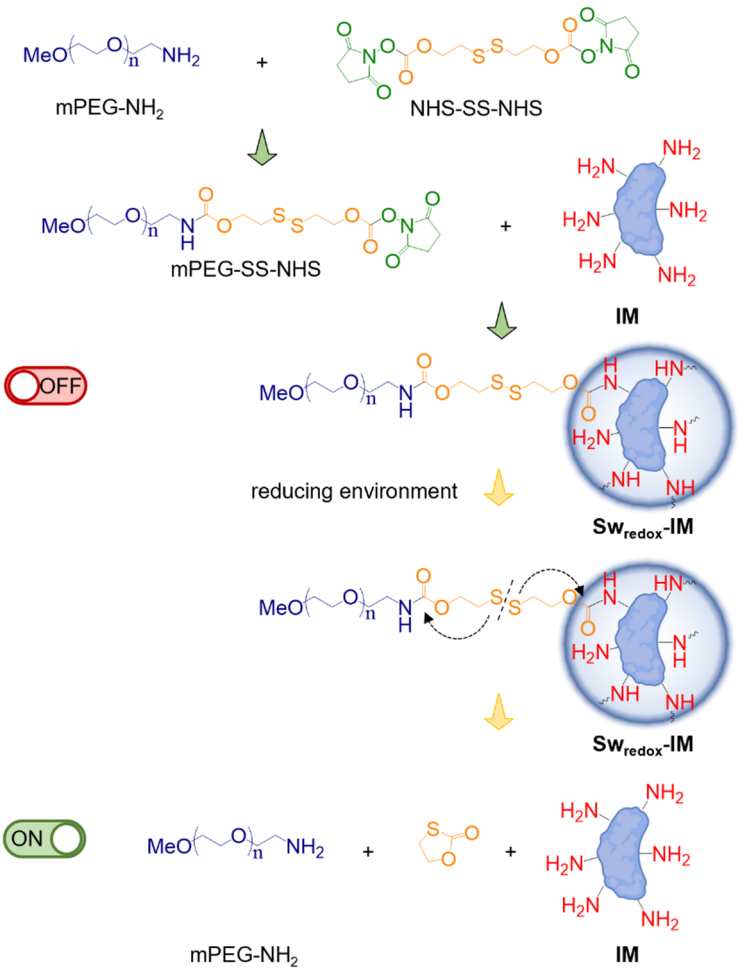

Fig. S1. Synthesis of redox-responsive switchable immune modulators (Sw_{redox}IMs) and selective switch on in the reducing environment. mPEG-NH_2, methoxy polyethylene glycol amine; NHS-SS-NHS, a redox-responsive linker bis(2,5-dioxopyrrolidin-1-yl) (disulfanediylbis(ethane-2,1-diyl)) dicarbonate.

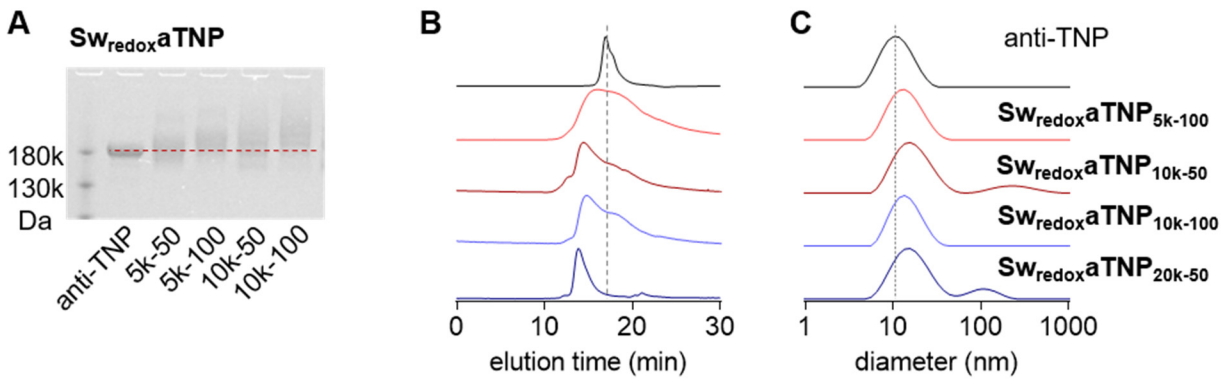

Fig. S2. Characterizations of Sw$_{redox}$aTNPs. (**A**) Sodium dodecyl sulfate-polyacrylamide gel electrophoresis (SDS-PAGE) characterizations of **Sw$_{redox}$aTNP**s. (**B**) Ultra high-performance liquid chromatography (UHPLC) traces of **Sw$_{redox}$aTNP**s with a size exclusion chromatography (SEC) column. (**C**) Hydrodynamic diameters of **Sw$_{redox}$aTNP**s measured by dynamic light scatting (DLS). Dash lines indicate the molecular weight (**A**), elution time (**B**), and hydrodynamic diameter (**C**) of native anti-trinitrophenal (TNP) antibody.

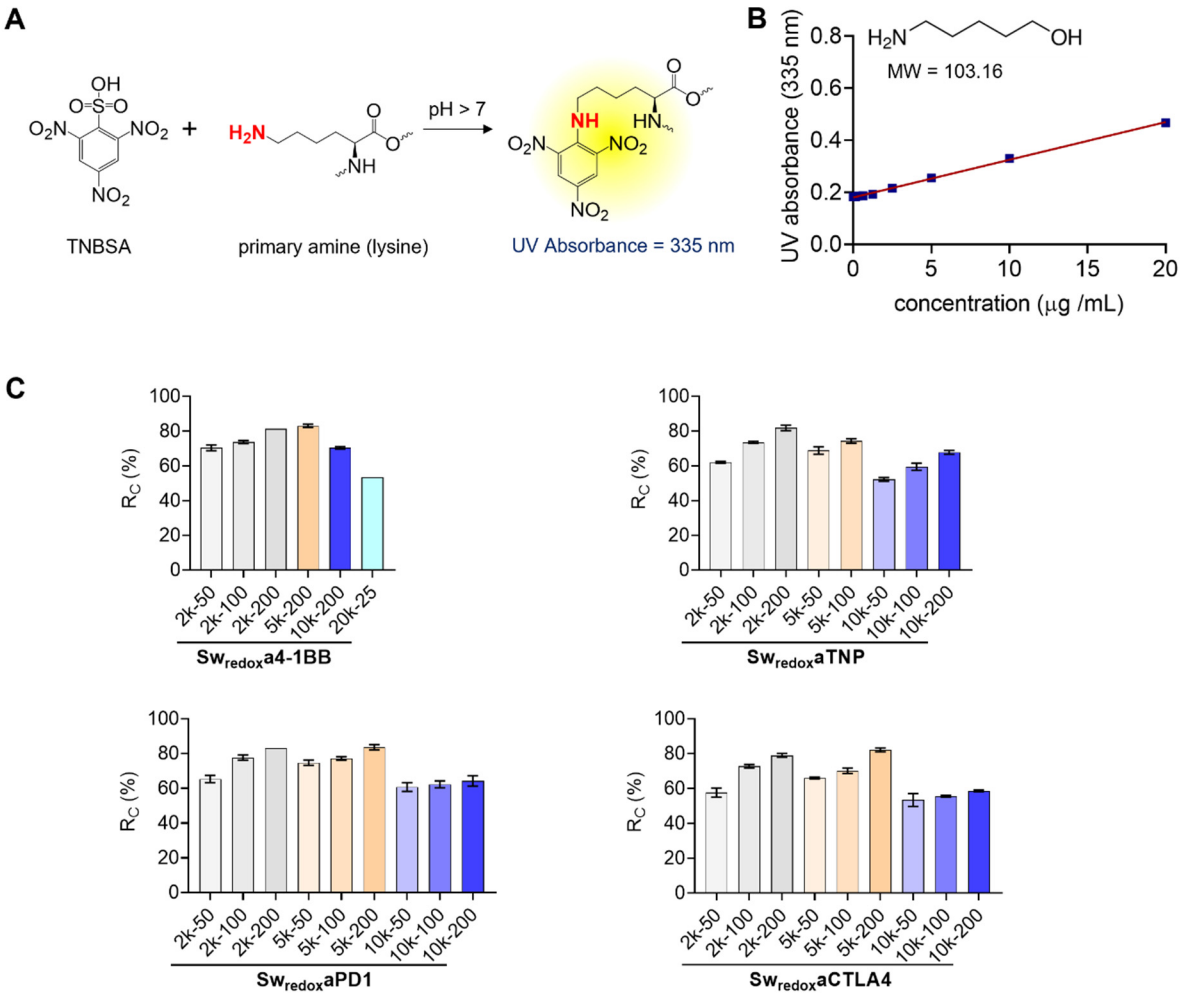

Fig. S3. Conjugation ratio (R_C) of Sw-IMs. (**A**) Schematic illustration of 2,4,6-trinitrobenzene sulfonic acid (TNBSA) assay for quantifying the number of primary amino groups. (**B**) Calibration curve using 5-amino-1-pentanol as a standard in TNBSA assay. (**C**) Conjugation ratio (R_C) of **Sw$_{redox}$a4-1BB**s, **Sw$_{redox}$aTNP**s, **Sw$_{redox}$aPD1**s, and **Sw$_{redox}$CTLA4**s. R_C defined as the percentage of PEG conjugated amino groups among all the detectable amino groups in the molecule.

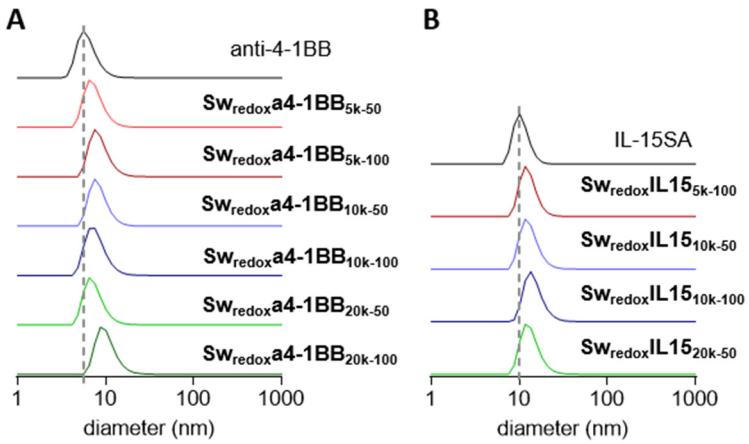

Fig. S4. DLS characterizations of Sw_{redox}IMs. (**A**) Hydrodynamic diameters of **Sw_{redox}a4-1BB**s. (**B**) Hydrodynamic diameters of **Sw_{redox}IL15**s. Dash lines indicate the size of the native antibody or cytokine.

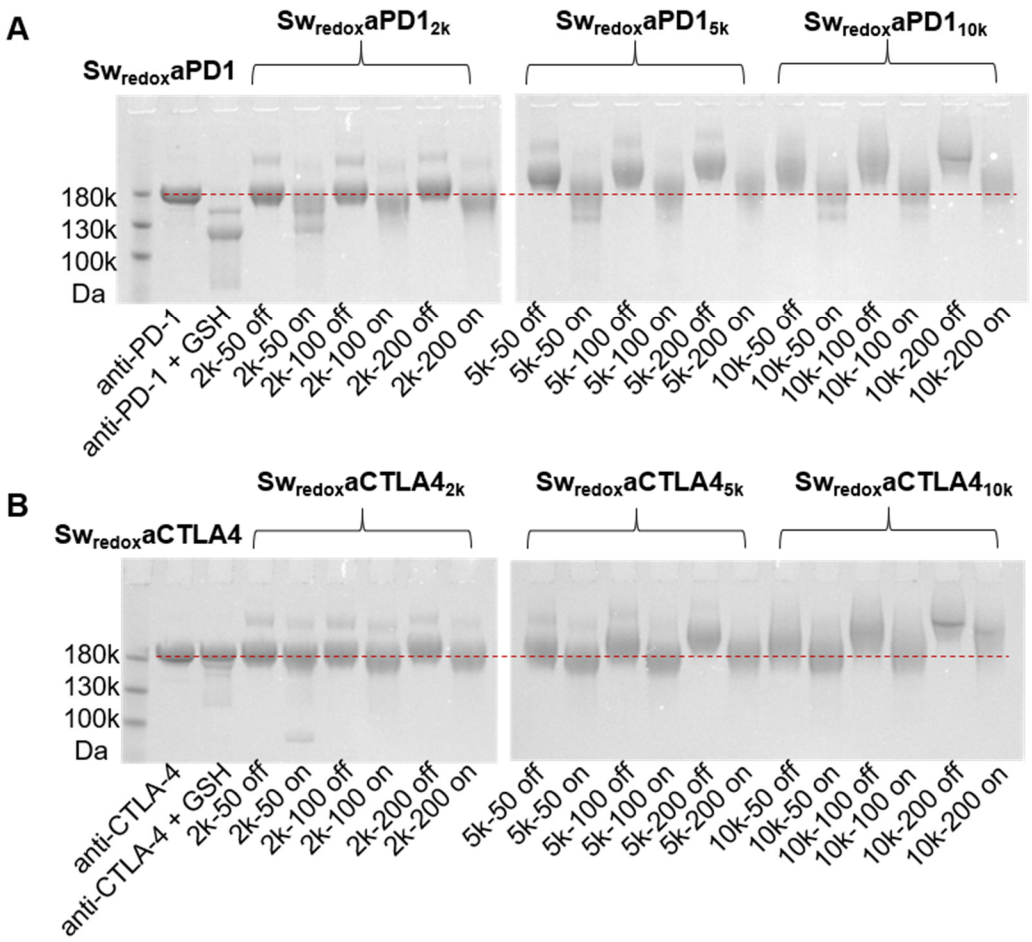

Fig. S5. SDS-PAGE characterizations of Sw$_{redox}$aPD1s (A) and Sw$_{redox}$aCTLA4s (B) at off and on status. Dash lines indicate the molecular weight of native antibodies.

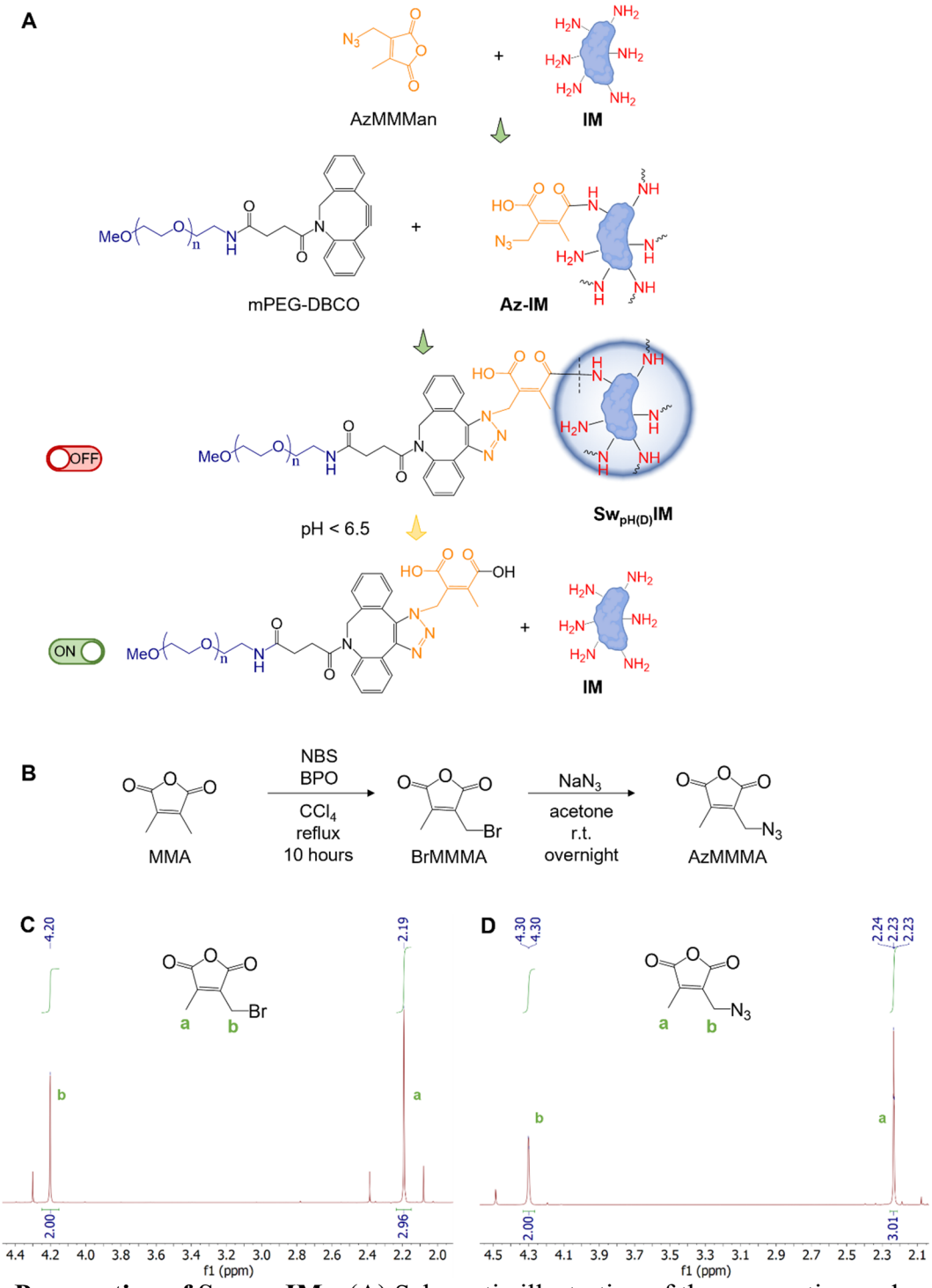

Fig. S6. Preparation of Sw$_{pH(D)}$IMs. (**A**) Schematic illustration of the preparation and switch on of **Sw$_{pH(D)}$IM**. mPEG-DBCO, dibenzocyclooctyne-functionalized mPEG; AzMMMan, (azidomethyl)methylmaleic anhydride; **Az-IM**, azido-functionalized **IM**. The dash line indicates the cleavable bond in acidic environment. (**B**) Synthesis of pH-responsive linker AzMMMan. (**C**) ^{1}H NMR spectrum of the intermediate product (bromomethyl)methylmaleic anhydride (BrMMMan), (400 MHz, $CDCl_3$) 4.20 (s, 2H, CH_2Br), 2.19 (s, 3H, CH_3). (**D**) ^{1}H NMR spectrum of AzMMMan, (400 MHz, $CDCl_3$) 4.29 (d, J < 1.0 Hz, 2H, CH_2N$_3$), 2.23 (t, J = 1.0 Hz, 3H, CH_3).

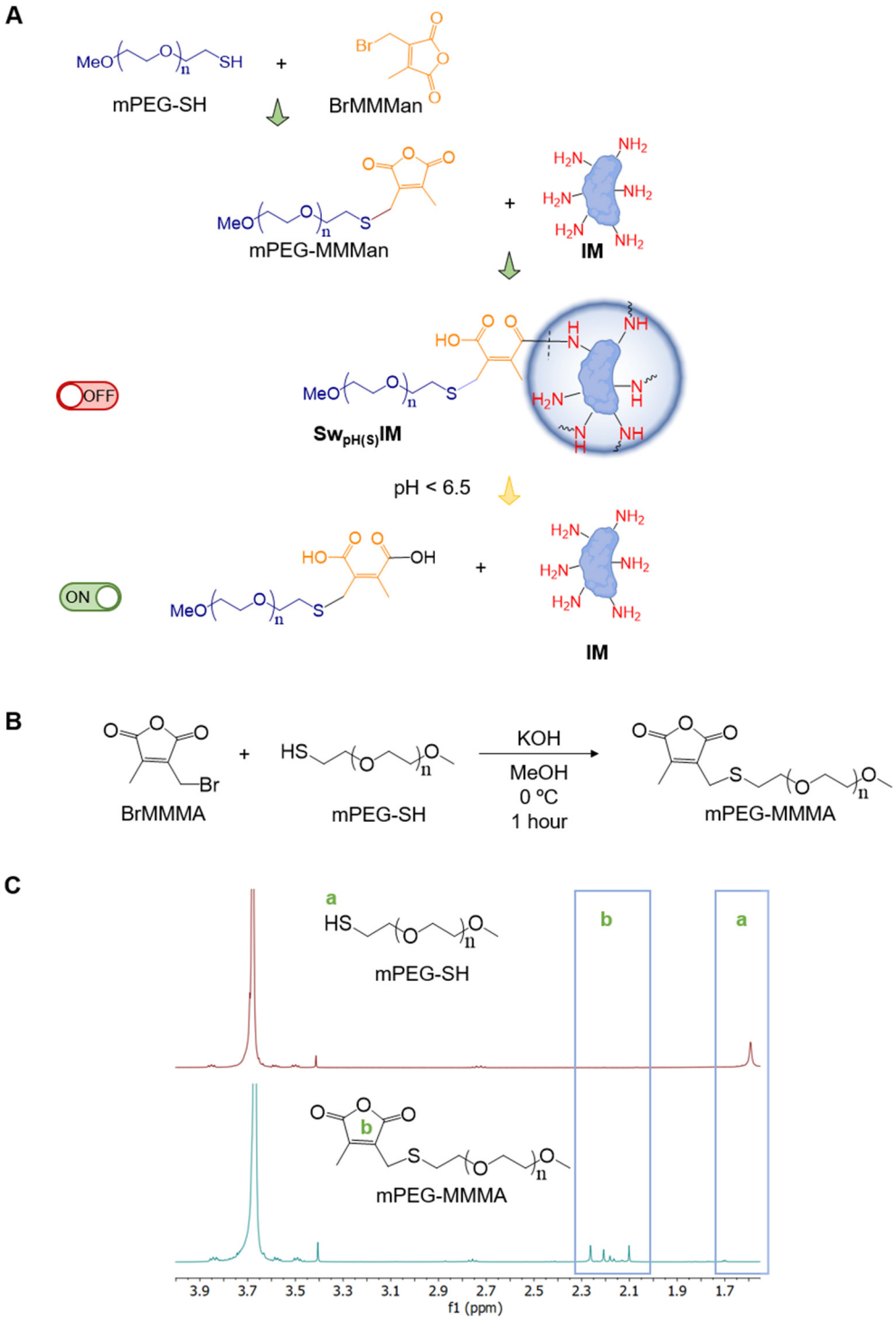

Fig. S7. Preparation of Sw$_{pH(S)}$IMs. (**A**) Schematic illustration of the preparation and switch on of **Sw$_{pH(S)}$IM**, mPEG-SH, mPEG thiol, the dash line indicates the cleavable bond in acidic environment. (**B**) Synthesis of MMA functionalized PEG, mPEG-MMMA. (**C**) ^{1}H NMR spectra of mPEG-SH and mPEG-MMMA. Blue boxes highlight the characteristic peaks of MMA moieties and thiol groups.

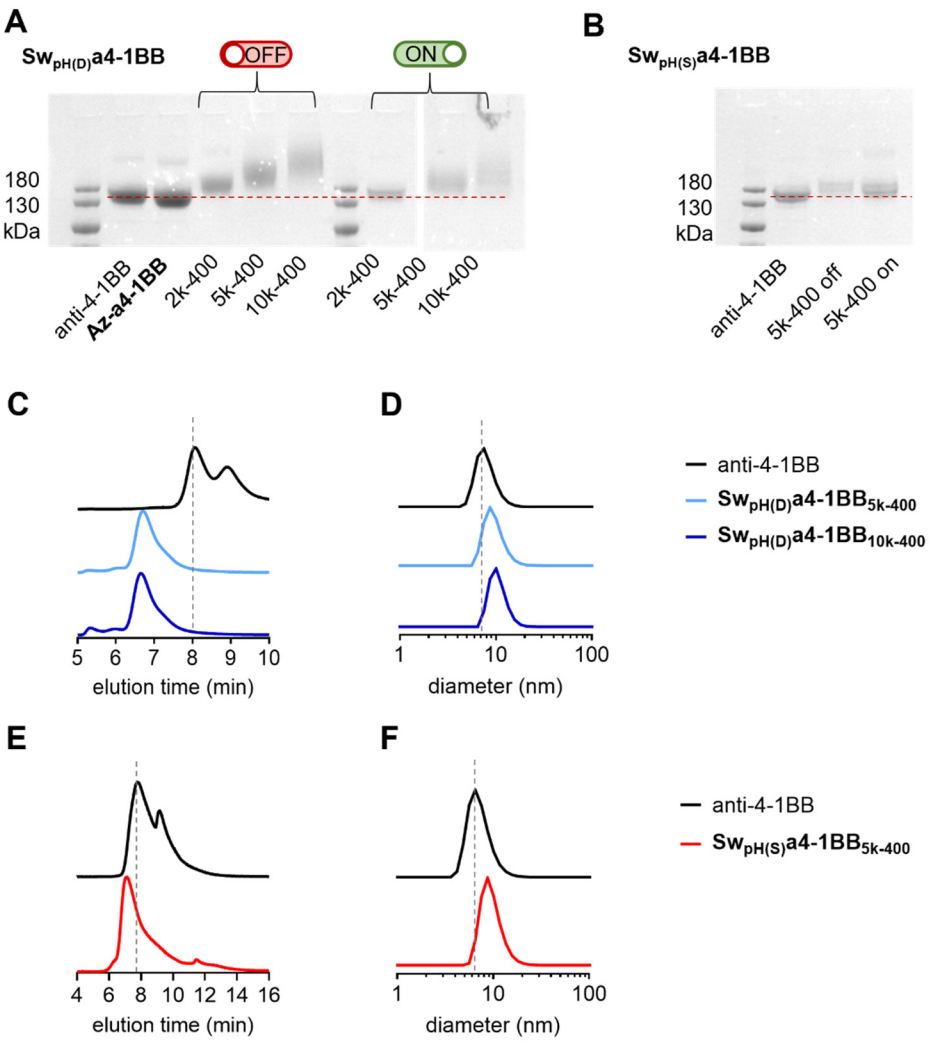

Fig. S8. Characterizations of acidic pH-responsive Sw-IMs. (**A**) SDS-PAGE characterization of **Sw$_{pH(D)}$a4-1BB**s at off and on status. **Az-a4-1BB**, azido-functionalized anti-4-1BB. (**B**) SDS-PAGE characterization of **Sw$_{pH(S)}$a4-1BB** at off and on status. (**C**) UHPLC-SEC traces of **Sw$_{pH(D)}$a4-1BB**s. (**D**) Hydrodynamic diameters of **Sw$_{pH(D)}$a4-1BB**s measured by DLS. (**E**) UHPLC-SEC traces of **Sw$_{pH(S)}$a4-1BB$_{5k-400}$**. (**F**) Hydrodynamic diameter of **Sw$_{pH(S)}$a4-1BB$_{5k-400}$** measured by DLS. Dash lines indicate the molecular weight, elution time, and hydrodynamic diameter of native anti-4-1BB.

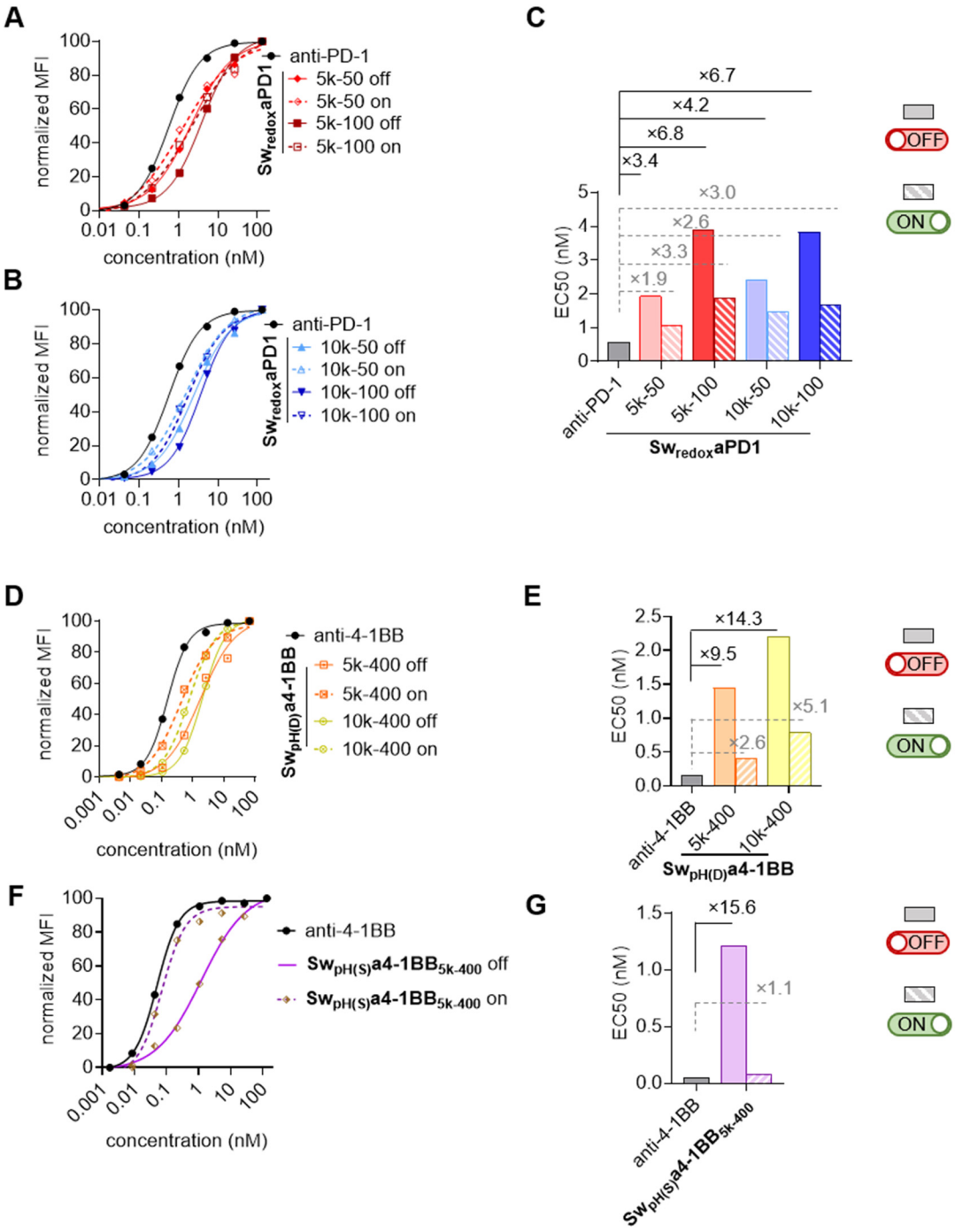

Fig. S9. Controlled switch off and on status of Sw-IMs characterized by a T cell binding assay. Activated $CD8^+$ T cells (1×10^5) were incubated with Alexa Fluor™647 (Alx-647)-labelled **Sw-IMs** at off or on status of series diluted concentrations for 1 hour. Mean fluorescent intensity (MFI) of Alx-647 on $CD8^+$ T cells was measured by flow cytometry to represent the binding capacity. **(A, B, D, F)** Binding capacity of **Sw-IMs** at off and on status with $CD8^+$ T cells. The plot of each formulation is a representative of three independent experiments. **(C, E, G)** The half maximal effective concentrations (EC50s) of **Sw-IMs** at off and on status.

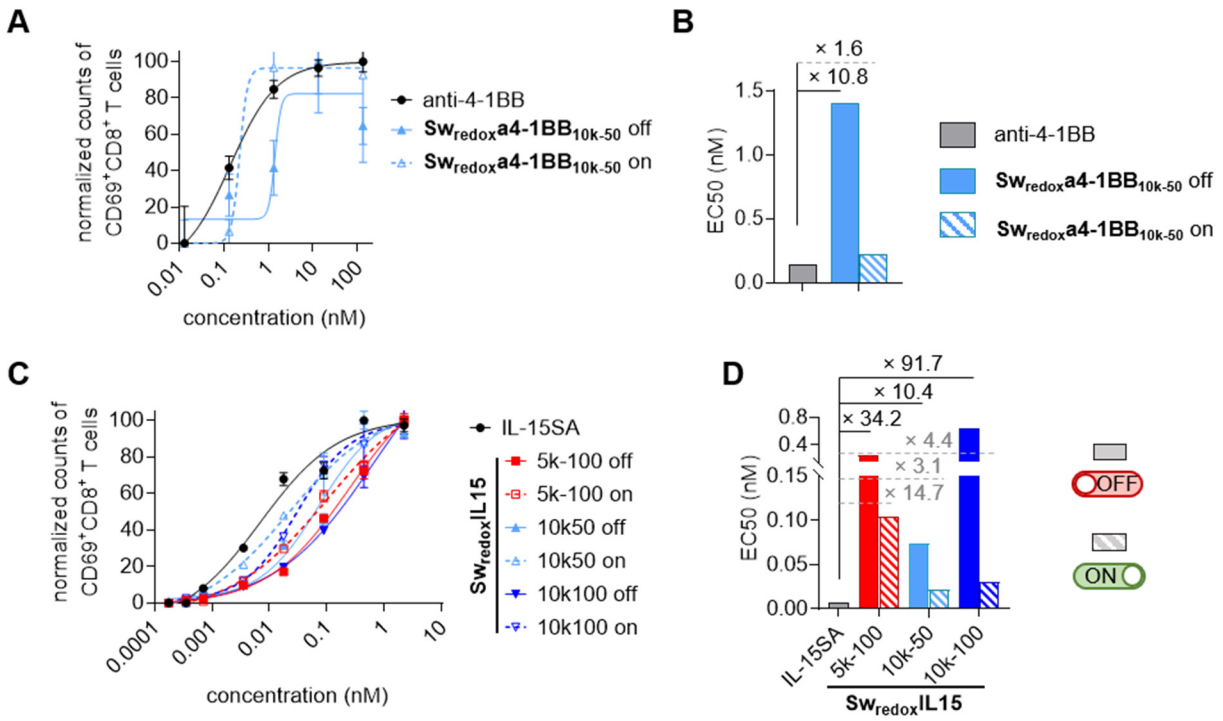

Fig. S10. Controlled switch off and on status of Sw-IMs characterized by a functional activity assay (**A**) Activities of **Sw$_{redox}$a4-1BB$_{10k-50}$** and native anti-4-1BB at off and on status in stimulating naïve CD8$^+$ T cells. (**B**) EC50s of **Sw$_{redox}$a4-1BB$_{10k-50}$** at off and on status. (**C**) Activities of **Sw$_{redox}$IL15**s and native IL-15SA at off and on status in stimulating CD8$^+$ T cells. (**D**) EC50s of **Sw$_{redox}$IL15**s at off and on status.

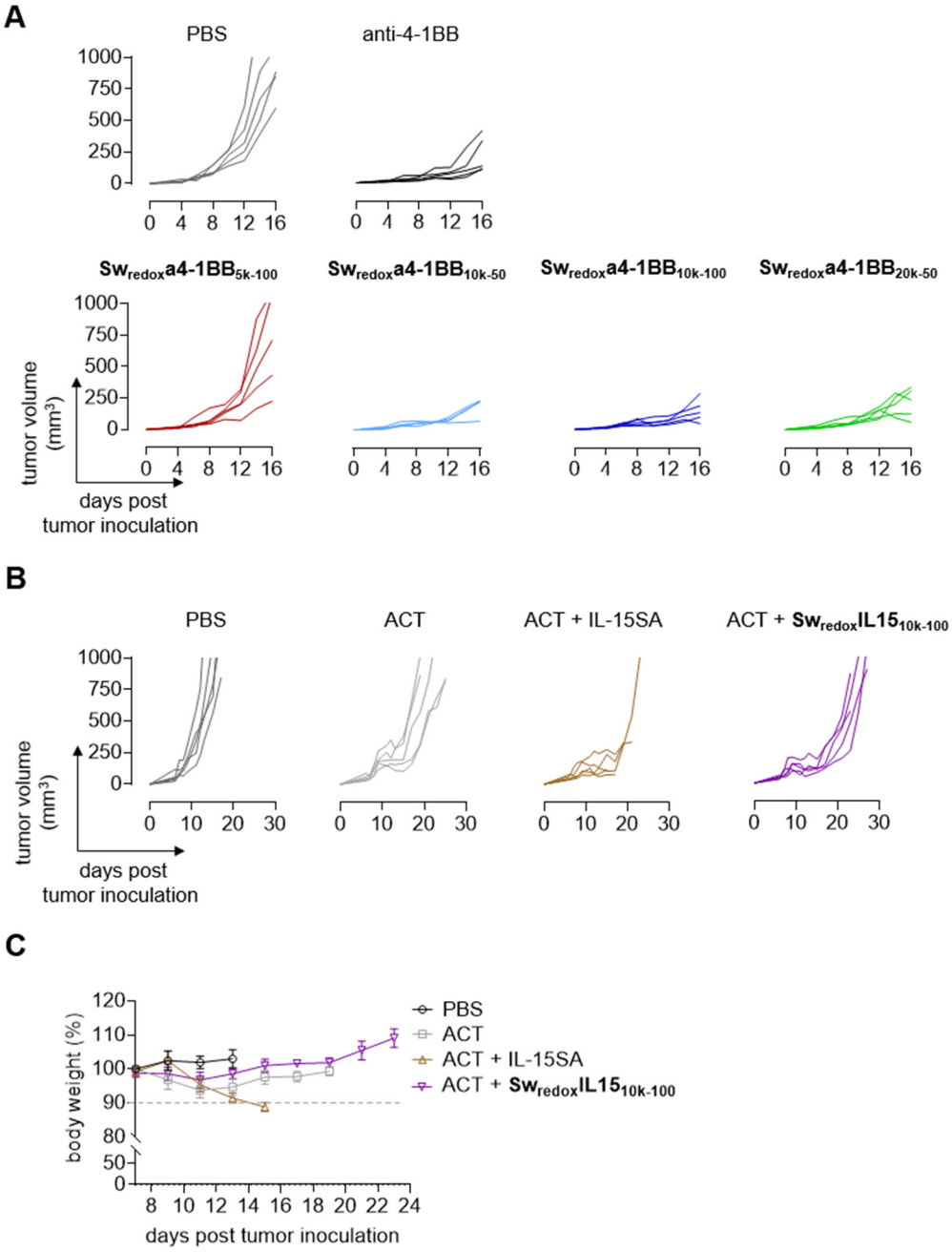

Fig. S11. Selective switch on of Sw-IMs in the tumor microenvironment leading to antitumor immunity. (**A**) C57BL/6 mice were inoculated subcutaneously (s.c.) with MC38 murine colon adenocarcinoma cells (2×10^5) and received intraperitoneal (i.p.) administration of native anti-4-1BB (100 μg), **Sw$_{redox}$a4-1BB**s (equivalent dose of anti-4-1BB), or PBS on day 4, 7, and 10 (n = 5 mice). Shown are individual tumor growth curves. (**B**, **C**) C57BL/6 mice were inoculated s.c. with B16F10 melanoma cells (5×10^5) and received adoptive transfer of activated Pmel Thy1.1$^+$CD8$^+$ T cells (1×10^7) on day 7 followed by intravenous (i.v.) administration of native IL-15SA (5 μg), **Sw$_{redox}$IL15$_{10k-100}$** (equivalent dose of IL-15SA), or PBS every other day from day 7 to day 21 (n = 5 mice). (**B**) Individual tumor growth curves. (**C**) Average body weight of the treated mice.

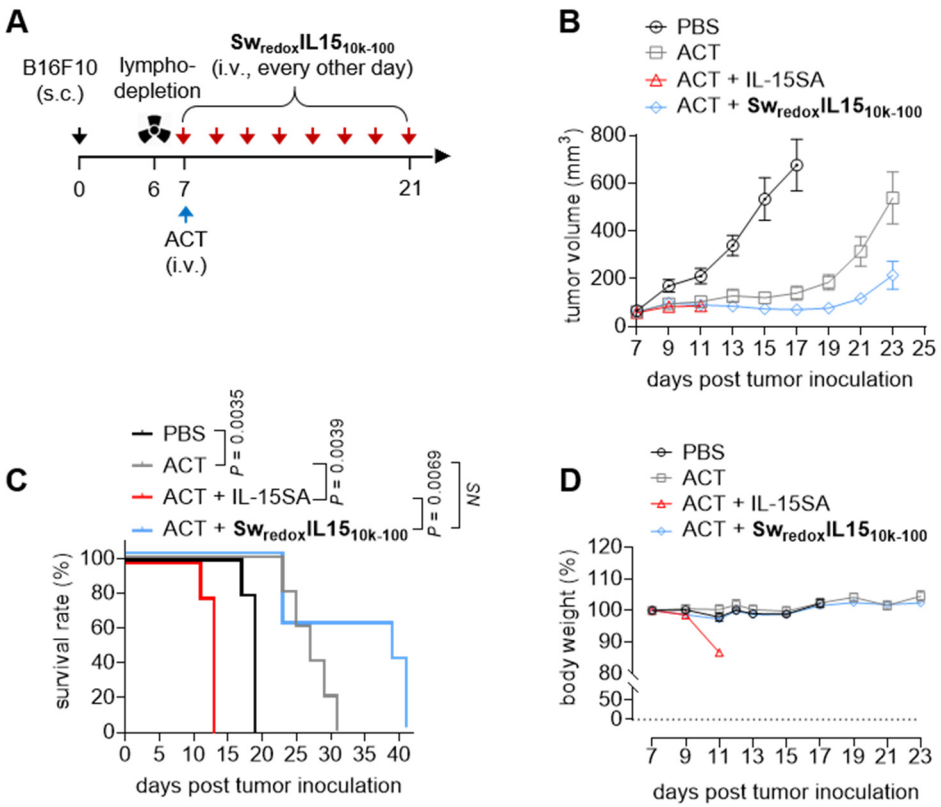

Fig. S12. Sw$_{redox}$IL15$_{10k-100}$ led to equivalent antitumor immunity but much enhanced safety compared to the native IL-15SA in adoptive T cell transfer (ACT) therapy with prior lymphodepletion. (**A**) C57BL/6 mice were inoculated s.c. with B16F10 cells (5×10^5) and received lymphodepletion (4 Gy) one day prior to the adoptive transfer of activated Pmel Thy1.1$^+$CD8$^+$ T cells (1×10^7) on day 7, which was followed by i.v. administration of native IL-15SA (10 μg), **Sw$_{redox}$IL15$_{10k-100}$** (equivalent dose of IL-15SA), or PBS every other day from day 7 to day 21 (n = 5 mice). (**B**) Average tumor growth curves. (**C**) Survival curves. (**D**) Average body weights. All data represent the mean ± s.e.m. and are analyzed by Log-rank test; *NS*, not significant ($P > 0.05$).

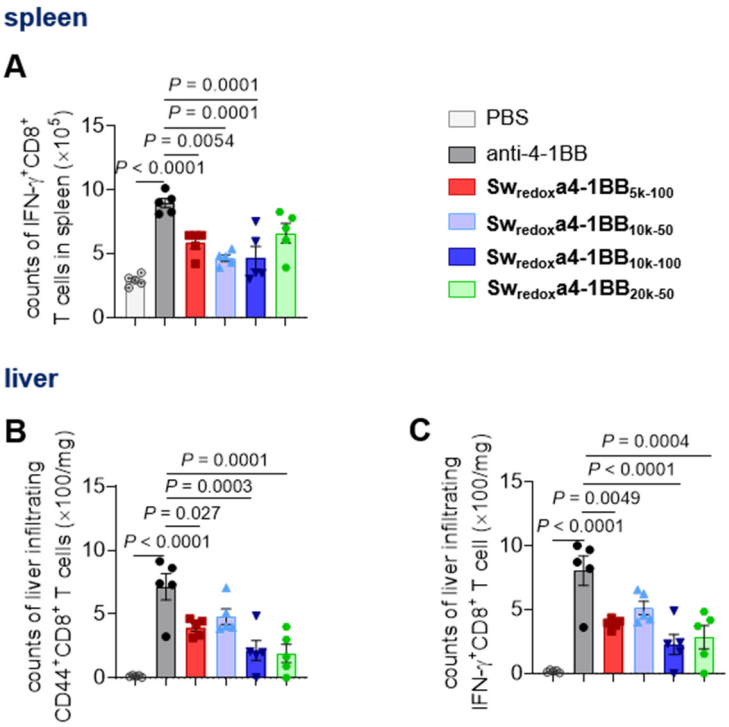

Fig. S13. Sw_{redox}a4-1BBs significantly reduced the toxicity of anti-4-1BB agonistic antibody therapy. C57BL/6 mice bearing MC38 colon adenocarcinoma were treated as shown in Fig. 3A. Mice were euthanatized on day 16 and the tissues were processed for histological and flow cytometry analyses (n = 5 mice). (**A**) Counts of IFN-γ-secreting $CD8^+$ T cells in spleen. (**B**) Counts of liver infiltrating $CD44^+CD8^+$ T cells. (**C**) Counts of liver infiltrating IFN-γ-secreting $CD8^+$ T cells. All data represent the mean ± s.e.m. and are analyzed by one-way ANOVA.

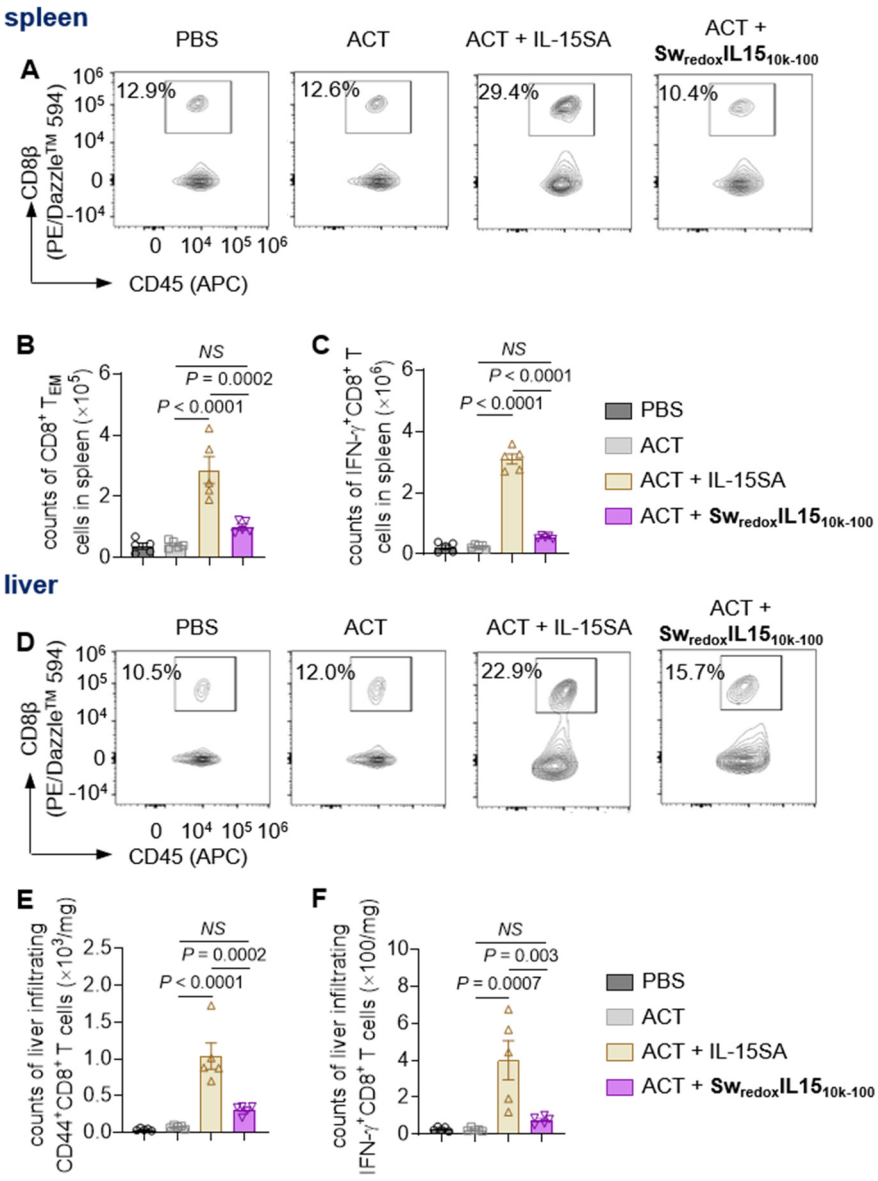

Fig. S14. Sw_{redox}IL15 markedly reduced the toxicity of the combination immunotherapy of IL-15SA and ACT. C57BL/6 mice were inoculated s.c. with B16F10 melanoma (5×10^5) and received adoptive transfer of Thy1.1$^+$CD8$^+$ T cells (1×10^7) on day 7 followed by i.v. administration of native IL-15SA (10 μg), **Sw_{redox}IL15$_{10k\text{-}100}$** (equivalent dose of IL-15SA), or PBS every other day from day 7 to day 13. Mice were euthanized on day 14 and the tissues were processed for flow cytometry analyses (n = 5 mice). (**A**) Representative flow cytometry plots of CD8$^+$ T cells among all lymphocytes (CD45$^+$) in spleen. (**B**) Counts of effector memory CD8$^+$ T cells (T_{EM}, CD44^{high}CD62L^{low}) in spleen. (**C**) Counts of IFN-γ-secreting CD8$^+$ T cells in spleen. (**D**) Representative flow cytometry plots of CD8$^+$ T cells among all liver infiltrating lymphocytes (CD45$^+$). (**E**) Counts of liver infiltrating CD44$^+$CD8$^+$ T cells. (**F**) Counts of liver-infiltrating IFN-γ-secreting T cells. All data represent the mean ± s.e.m. and are analyzed by one-way ANOVA; *NS*, not significant ($P > 0.05$).

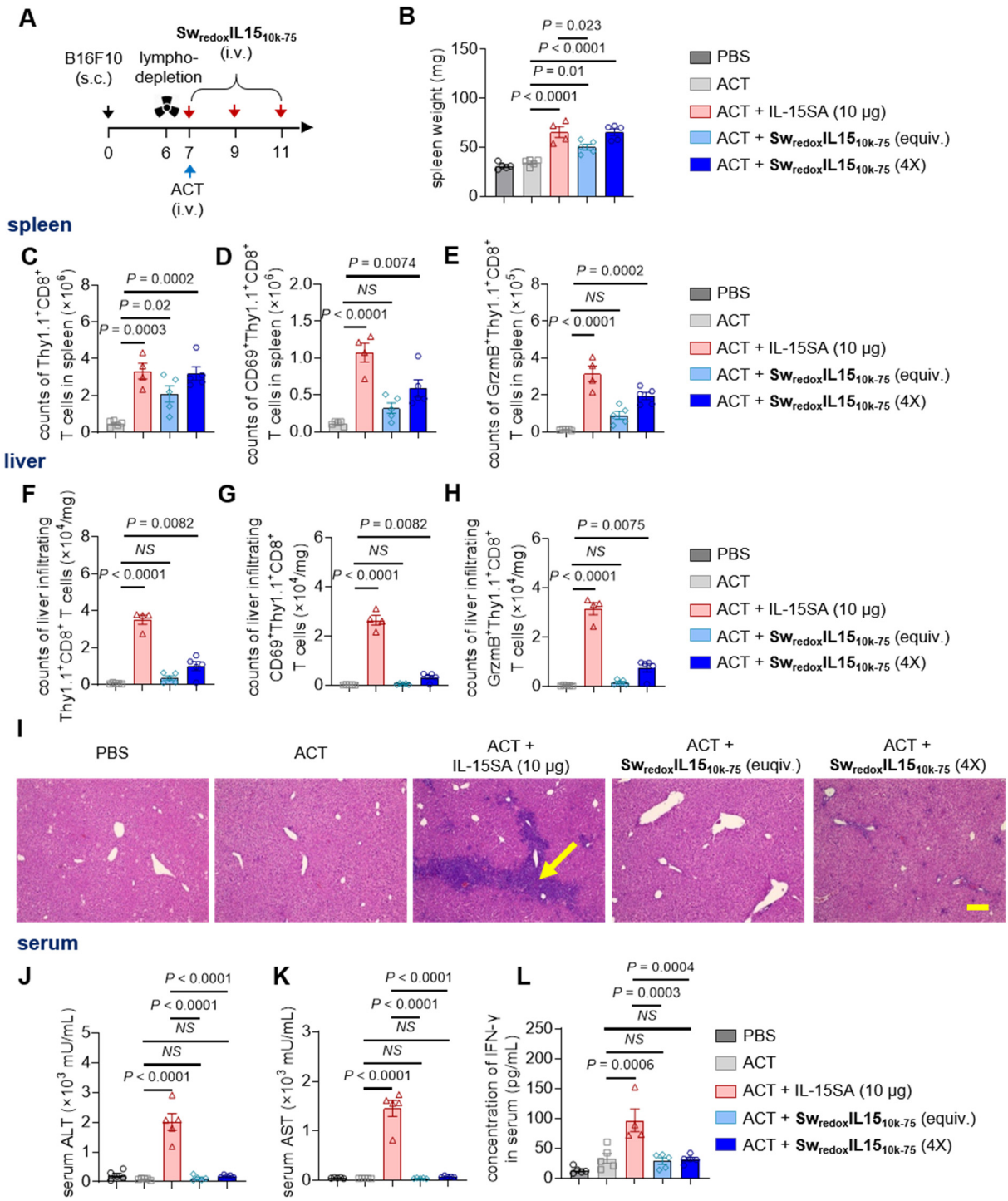

Fig. S15. Sw$_{redox}$IL15 markedly reduced the toxicity of the combination immunotherapy of IL-15SA and ACT with prior lymphodepletion. (**A**) C57BL/6 mice were inoculated s.c. with B16F10 melanoma (5×10^5) and received lymphodepletion (4 Gy) one day prior to the adoptive transfer of activated Pmel Thy1.1$^+$CD8$^+$ T cells (1×10^7) on day 7, which was followed by i.v. administration of native IL-15SA (10 μg), **Sw$_{redox}$IL15$_{10k-75}$** (equivalent dose of IL-15SA), **Sw$_{redox}$IL15$_{10k-75}$** (4× dose of IL-15SA), or PBS on day 7, 9, and 11. Mice were euthanized on

day 12 and the tissues were processed for flow cytometry and histological analyses (n = 5 mice). (**B**) Average spleen weight. (**C**) Counts of $Thy1.1^{+}CD8^{+}$ T cells in spleen. (**D**) Counts of $CD69^{+}Thy1.1^{+}CD8^{+}$ T cells in spleen. (**E**) Counts of GrzmB-secreting $Thy1.1^{+}CD8^{+}$ T cells in spleen. (**F**) Counts of liver infiltrating $Thy1.1^{+}CD8^{+}$ T cells. (**G**) Counts of liver infiltrating $CD69^{+}Thy1.1^{+}CD8^{+}$ T cells. (**H**) Counts of liver infiltrating GrzmB-secreting $Thy1.1^{+}CD8^{+}$ T cells. (**I**) Histopathological analyses of liver tissues. Yellow arrows indicate tissue damage. Scale bar, 200 μm. (**J**) Serum activity of alanine aminotransferase (ALT). (**K**) Serum activity of aspartate transaminase (AST). (**L**) Serum concentration of IFN-γ. All data represent the mean ± s.e.m. and are analyzed by one-way ANOVA; *NS*, not significant ($P > 0.05$).

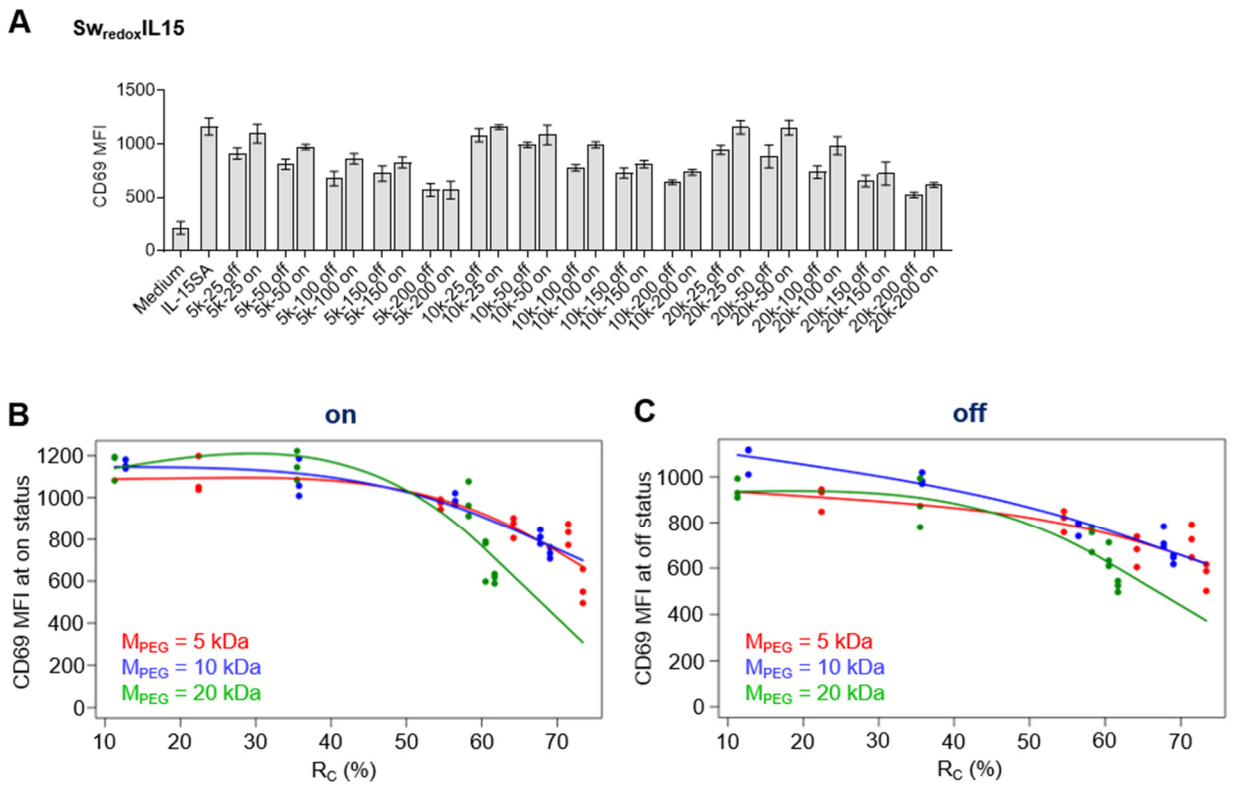

Fig. S16. In vitro T cell activation by Sw$_{redox}$IL15s of different formulations. (**A**) MFI of CD69 expressed by CD8$^+$ T cells cultured with **Sw$_{redox}$IL15**s at off and on status or native IL-15SA. (**B**, **C**) Plots of CD69 MFI of **Sw$_{redox}$IL15**s with different M_{PEG} at off and on status as functions of R_C. Smooth curves were obtained using penalized cubic regression splines.

Table S1. Preparation of Sw-IMs of various formulations.

Entry	Sw-IM*	IM	linker†	M_{PEG}‡ (Da)	R_F§	R_C‖ (%)
1	$Sw_{redox}aTNP_{2k\text{-}50}$	anti-TNP	SS	2k	50	62.1
2	$Sw_{redox}aTNP_{2k\text{-}100}$	anti-TNP	SS	2k	100	73.6
3	$Sw_{redox}aTNP_{2k\text{-}200}$	anti-TNP	SS	2k	200	81.9
4	$Sw_{redox}aTNP_{5k\text{-}50}$	anti-TNP	SS	5k	50	68.9
5	$Sw_{redox}aTNP_{5k\text{-}100}$	anti-TNP	SS	5k	100	74.3
6	$Sw_{redox}aTNP_{10k\text{-}50}$	anti-TNP	SS	10k	50	52.3
7	$Sw_{redox}aTNP_{10k\text{-}200}$	anti-TNP	SS	10k	200	67.8
8	$Sw_{redox}a4\text{-}1BB_{2k\text{-}50}$	anti-4-1BB	SS	2k	50	47.7
9	$Sw_{redox}a4\text{-}1BB_{2k\text{-}100}$	anti-4-1BB	SS	2k	100	52.8
10	$Sw_{redox}a4\text{-}1BB_{2k\text{-}200}$	anti-4-1BB	SS	2k	200	56.6
11	$Sw_{redox}a4\text{-}1BB_{5k\text{-}200}$	anti-4-1BB	SS	5k	200	83.1
12	$Sw_{redox}a4\text{-}1BB_{10k\text{-}200}$	anti-4-1BB	SS	10k	200	80.4
13	$Sw_{redox}a4\text{-}1BB_{20k\text{-}25}$	anti-4-1BB	SS	20k	25	53.5
14	$Sw_{redox}aPD1_{2k\text{-}50}$	anti-PD-1	SS	2k	50	65.4
15	$Sw_{redox}aPD1_{2k\text{-}100}$	anti-PD-1	SS	2k	100	77.7
16	$Sw_{redox}aPD1_{2k\text{-}200}$	anti-PD-1	SS	2k	200	83.2
17	$Sw_{redox}aPD1_{5k\text{-}50}$	anti-PD-1	SS	5k	50	74.7
18	$Sw_{redox}aPD1_{5k\text{-}100}$	anti-PD-1	SS	5k	100	77.2
19	$Sw_{redox}aPD1_{5k\text{-}200}$	anti-PD-1	SS	5k	200	83.6
20	$Sw_{redox}aPD1_{10k\text{-}50}$	anti-PD-1	SS	10k	50	60.8
21	$Sw_{redox}aPD1_{10k\text{-}200}$	anti-PD-1	SS	10k	200	64.3
22	$Sw_{redox}aCTLA4_{2k\text{-}50}$	anti-CTLA-4	SS	2k	50	57.7
23	$Sw_{redox}aCTLA4_{2k\text{-}100}$	anti-CTLA-4	SS	2k	100	72.9
24	$Sw_{redox}aCTLA4_{2k\text{-}200}$	anti-CTLA-4	SS	2k	200	79.1
25	$Sw_{redox}aCTLA4_{5k\text{-}50}$	anti-CTLA-4	SS	5k	50	66.0
26	$Sw_{redox}aCTLA4_{5k\text{-}100}$	anti-CTLA-4	SS	5k	100	70.2
27	$Sw_{redox}aCTLA4_{5k\text{-}200}$	anti-CTLA-4	SS	5k	200	82.2
28	$Sw_{redox}aCTLA4_{10k\text{-}50}$	anti-CTLA-4	SS	10k	50	53.5
29	$Sw_{redox}aCTLA4_{10k\text{-}200}$	anti-CTLA-4	SS	10k	200	58.7
30	$Sw_{redox}IL15_{5k\text{-}25}$	IL-15SA	SS	5k	25	22.4
31	$Sw_{redox}IL15_{5k\text{-}50}$	IL-15SA	SS	5k	50	54.5
32	$Sw_{redox}IL15_{5k\text{-}150}$	IL-15SA	SS	5k	150	71.5
33	$Sw_{redox}IL15_{5k\text{-}200}$	IL-15SA	SS	5k	200	73.4
34	$Sw_{redox}IL15_{10k\text{-}25}$	IL-15SA	SS	10k	25	12.7
35	$Sw_{redox}IL15_{10k\text{-}75}$	IL-15SA	SS	10k	75	49.5
36	$Sw_{redox}IL15_{10k\text{-}150}$	IL-15SA	SS	10k	150	67.7
37	$Sw_{redox}IL15_{10k\text{-}200}$	IL-15SA	SS	10k	200	69.0
38	$Sw_{redox}IL15_{20k\text{-}25}$	IL-15SA	SS	20k	25	11.3
39	$Sw_{redox}IL15_{20k\text{-}100}$	IL-15SA	SS	20k	100	58.2
40	$Sw_{redox}IL15_{20k\text{-}150}$	IL-15SA	SS	20k	150	60.5

41	**$Sw_{redox}IL15_{20k\text{-}200}$**	IL-15SA	SS	20k	200	61.7
42	**$Sw_{pH(D)}a4\text{-}1BB_{2k\text{-}400}$**	anti-4-1BB	DBCO	2k	400	
43	**$Sw_{pH(D)}a4\text{-}1BB_{10k\text{-}400}$**	anti-4-1BB	DBCO	10k	400	

*__Sw-IM__, switchable immune modulator. **Sw-IM** is denoted as **$Sw_{linker}protein_{MPEG\text{-}RF}$**. **redox**, redox-responsive linker; **pH(D)**, acidic pH-responsive linker with a DBCO-triazole spacer; **aTNP**, anti-TNP antibody; **a4-1BB**, anti-4-1BB antibody; **aPD1**, anti-PD-1 antibody; **aCTLA4**, anti-CTLA-4 antibody; **IL15**, IL-15SA.

†The chemical structure of the linkers is shown in Fig. 1. SS, disulphate linker; DBCO, dibenzocyclooctyne.

‡M_{PEG}, molecular weight of polyethylene glycol (PEG).

§R_F, feeding mole ratio of PEG to **IM**.

‖R_C, conjugation ratio, defined as (number of conjugated NH_2 groups / total number of NH_2 groups of **IM**) × 100%.